Results in Physics 19 (2020) 103428

Contents lists available at ScienceDirect

Results in Physics

journal homepage: www.elsevier.com/locate/rinp

GaN and InGaN nanowires prepared by metal-assisted electroless etching: Experimental and theoretical studies

S. Assa Aravindh [a,b], Bin Xin [a], Somak Mitra [a], Iman S. Roqan [a,*], Adel Najar [c,*]

[a] King Abdullah University of Science and Technology, Physical Science and Engineering (PSE) Division, Thuwal 23955-6900, Saudi Arabia
[b] Nano and Molecular Systems Research Unit, University of Oulu, P.O. Box 8000, FI-90014 Oulu, Finland
[c] Department of Physics, College of Science, United Arab Emirates University, Al Ain 15551, United Arab Emirates

ARTICLE INFO

Keywords:
GaN
InGaN
Nanowires
DFT
Electronic structure

ABSTRACT

We investigate the optical and structural properties of GaN and InGaN nanowires (NWs) fabricated by metal-assisted electroless etching in a hydrofluoric acid (HF) solution. The emission spectra of GaN and InGaN NWs exhibit a red shift compared to the as-grown samples resulting from an increase in the surface-to-volume ratio and stress relaxation in these nanostructures. The carrier lifetimes of GaN and InGaN NWs were measured. In addition, density functional theory (DFT) investigations were carried out on GaN and InGaN NWs using the generalized gradient approximation (GGA), including the Hubbard *U* parameter. The presence of compressive stress in the NWs was confirmed by the DFT calculations, which indicated that it induces a change in the lattice parameter along the c-direction. Formation energy calculations showed that In is a much more stable dopant in the GaN NWs compared to the native point defects, such as Ga and N vacancies. Moreover, electronic structure analysis revealed that the complex defects formed by the presence of In along with vacancy defects shifts the valence band maximum, thus changing the conducting properties of the NWs.

Introduction

Nanowires (NWs) are promising semiconductors nanostructure for next-generation electronics, photonics, sensors, and energy devices [1–6]. NWs have a large surface-to-volume ratio [7] and 1D structure that shows the possibility of investigating quantum confinement effects and surface-mediated phenomena, which strongly affect the physical properties of these nanostructures. In addition, compared to quantum dots, it is more challenging compare to planar structures to develop contact electrodes for NWs required for building active devices, as well as for forming interconnects or waveguides [8–12] GaN and InGaN materials are particularly important compound semiconductors due to their direct band gaps [13]. As band gap can be tuned, this property facilitates the fabrication of optoelectronic compounds working in the UV–Vis-IR regions [14–16]. 1D structure of GaN and InGaN materials reduce mechanical strain [17] and enhanced In composition in InGaN [18]. Furthermore, the nanowire has low dislocation density depending on the fabrication methods and low non-radiative recombination centers leading to improve of radiative efficiency [19,20]. NWs have higher surface-to-volume ratio, this increases the density of surface states, which are non-radiative centers. Also, the extraction of light will be enhanced due to the significant increase in surface-to-volume ratio inherent in the nanostructure geometry [5,21–26]. In the extant studies in this field, strategies used for preparation of GaN or InGaN based NWs tend to rely on molecular beam epitaxy [27,28], chemical vapor deposition (CVD) [29,30], hybrid vapor epitaxy [31,32], and selective area epitaxy [33,34]. However, in recent years, metal-assisted electroless etching for silicon NW synthesis was developed [35,36]. Recently, researchers explored the synthesis of GaN and InGaN NWs by metal-assisted electroless etching [37–39]. However, the optical and related electronic properties of this material have not been studied yet.

In this work, we synthesized GaN and InGaN NWs using metal-assisted electroless etching and subsequently studied their morphology and optical properties. In addition, the density functional theory (DFT) based simulations was employed to support the experimental investigations and study the effect on the optical properties of introducing In in the GaN NW structure. DFT simulations have become an essential tool in predicting experimental phenomena in semiconductor NWs [40]. Moreover, theoretical studies focusing on the role of defects and impurities in GaN NWs is helpful to explain the experimental findings [41–43] related to the InN cluster formation. In the present investigation, we focused on substitutional In doping into the Ga sites, as well as

* Corresponding authors.
E-mail addresses: iman.roqan@kaust.edu.sa (I.S. Roqan), adel.najar@uaeu.ac.ae (A. Najar).

https://doi.org/10.1016/j.rinp.2020.103428
Received 19 June 2020; Received in revised form 18 September 2020; Accepted 19 September 2020
Available online 24 September 2020

the induction of native point defects, such as Ga and N vacancies. Defect stability was assessed through formation energy calculations, whereas electronic structure analysis was carried out to gain insight into the experimental observations.

Methods

Samples preparation and characterization

The unintentionally commercial Si doped n-type GaN epilayer film and undoped $In_xGa_{1-x}N$ epitaxy grown on Si doped n-type GaN used in this study were purchased from Xim. Powerway Adv. Material Co Ltd. GaN sample has a resistivity of 0.05 Ω.cm and a thickness of about 30 μm. The thickness of $In_xGa_{1-x}N$ (x = 0.2) sample is 400 nm thickness. The structures of GaN and InGaN samples used in this study were presented in Fig. 1(a). Before NW synthesis, GaN and InGaN substrates were cleaned by sonication for 5 min each in acetone and 2-propanol. Then, the samples were immersed in HNO_3 at 65 °C for 15 min before being rinsed in deionized (DI) water and methanol. Following the cleaning process, two narrow strips of 10-nm-thick Pt, separated by a 5 mm, were deposited on the GaN and InGaN samples using a sputtering system. The NWs were synthesized using metal-assisted electroless etching method in a H_2O_2:HF:CH_3OH (2:1:2) solution under UV illumination for 180 min and 30 min, respectively for GaN and InGaN samples. The optimized etching duration was adopted, as reported previously [36,37]. After chemical etching, the samples were removed from the solution and rinsed with DI water.

The sample morphologies were analysed using a JEOL scanning electron microscope (SEM), and X-ray measurements (XRD) were performed on a Bruker D8 Advance system. The photoluminescence (PL) measurements were performed at room temperature (RT) using a He-Cd laser of 20 mW power emitting at 325 nm. Time-resolved photoluminescence (TRPL) was performed using a third harmonic line of 266 nm (obtained by APE-SHG/THG) of the Coherent Mira 900 Ti:sapphire femtosecond laser (using fundamental line of 800 nm and 75 MHz repetition rate) was used for excitation. To detect the TRPL signal, the streak camera (Hamamatsu C6860) was employed using syncroscan mode with ~ 2 ps resolution [44,45]. RT absorption measurements were carried out using UV–vis Varian Cary 5000 spectrophotometry. A 900 W xenon lamp was used for PL excitation (PLE) measurements at RT, using Edinburgh Instruments FLS980 spectrometer.

Computational methodology

The DFT simulations were carried out using the plane wave code Vienna Ab initio Simulation Package (VASP) including spin polarization [46]. The $Ga_{48}N_{48}$ NW was modelled along the hcp [0001] orientation with a supercell length of 2c, such that the simulation cell contained four GaN atomic layers with 96 atoms [46]. A vacuum of ~20 Å was used along the X and Y directions to ensure negligible interaction between the periodically repeated NW images, whereas infinite periodicity was maintained along the Z-direction. A plane wave cut-off energy of 400 eV and pseudo-potentials with projected augmented wave basis were adopted. The exchange and correlations were described using generalized gradient approximation (GGA) in the Perdew Burke–Ernzerhof (PBE) form [47]. The convergence criteria for energy and force tolerances were 0.0001 eV and 0.004 eV/Å, respectively, which are sufficient enough to minimize the Hellmann-Feynman forces. Monkhorst pack k-grid with dimensions of (1 × 1 × 8) dimensions was used for Brillouin zone integration. Since standard DFT is inadequate for describing the GaN electronic structure because of strong electronic correlations of the 3d electrons, in this work, GGA + U method was employed. The on-site Coulomb parameters used for Ga were U = 6.7 eV and J = 0.7 eV [48], as implemented in VASP.

Results and discussion

Experimental results

The etched samples were analysed by SEM, and the resulting images are presented in Fig. 1(b)-(d). As shown in Fig. 1(b), the samples etched for 180 min present a high density of NWs. The shorter NWs are

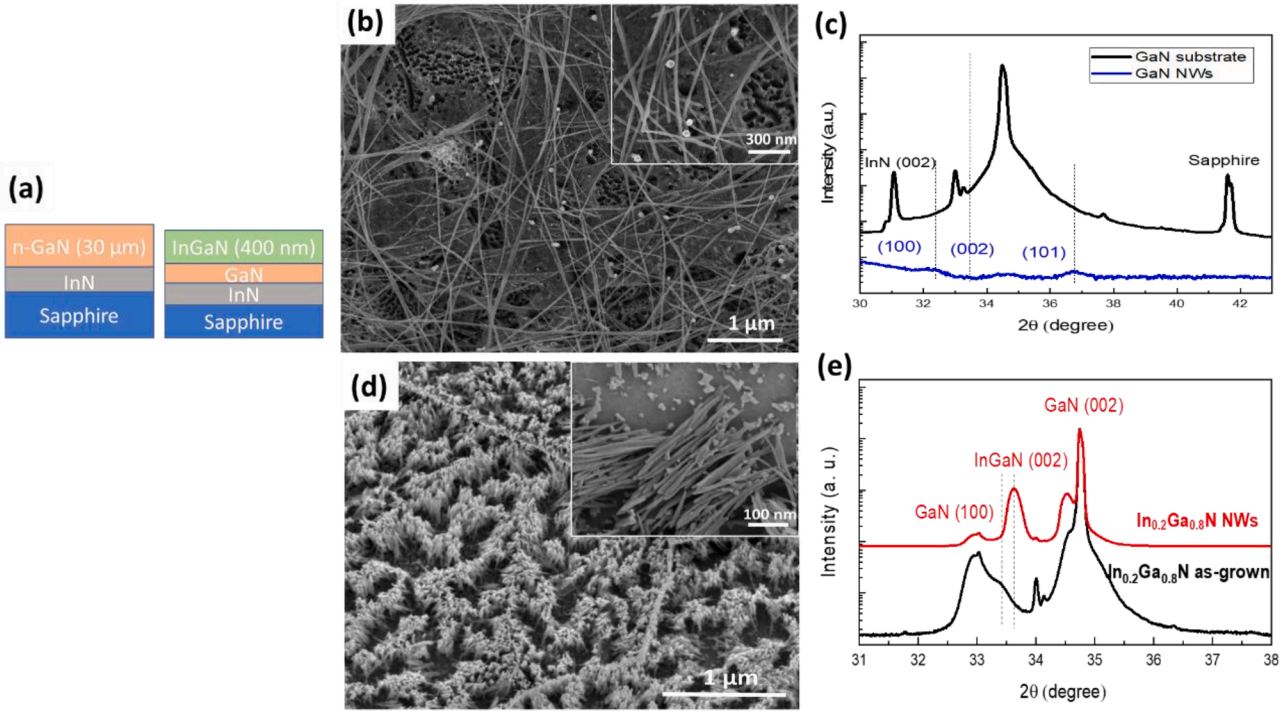

Fig. 1. (a) Schematic diagram showing GaN and InGaN structures used to synthesise nanowires by metal-assisted electroless etching. (b)-(c) SEM image and X-ray diffraction profiles of wurtzite GaN NWs etched for 180 min. (d)-(e) SEM image and X-ray diffraction profiles of InGaN NWs etched for 30 min and as-grown InGaN.

vertically oriented and are supported by the underlying nano-porous GaN structures. The GaN NWs diameter and length are about 35 nm and 1–13 μm, respectively, as shown in the inset of Fig. 1(b). However, a vertical oriented InGaN NWs in Fig. 1(d) are observed for the sample etched for 30 min with length about 280 nm (inset in Fig. 1(d)).

The X-ray diffraction (XRD) measurements were performed on GaN and InGaN NWs to study the structural properties of the NWs. Fig. 1(c) show the diffraction peaks of GaN NWs and the as-grown GaN, the peaks for GaN NWs are located at 2θ = 32.4°, 34.6°, 36.7°, corresponding to (1 0 0), (0 0 2) and (1 0 1) lattice planes, respectively. This structure is corresponding to wurtzite GaN (JCPDS card No: 898624) with lattice constants a = 0.3186 nm and c = 0.5178 nm. The angle of the XRD (0 0 2) peak of the nanowires presented a small shift compared to the as-grown sample (34.5), which due to the compressive stress relaxation [49].

Fig. 1(e) show the XRD measurements of as-grown InGaN and InGaN samples etched for 30 min. The identified planes GaN (1 0 0) and GaN (0 0 2) are corresponding to the diffraction peaks located at 32.9° and 34.7°, respectively. However, the planes InGaN (0 0 2) is located at 2θ = 33.4° for the as-grown and 33.6° for the InGaN nanowires. This shift can be explained by the relaxation of compressive stress after etching. The decrease of dislocation defects at the surface during etching lead to smaller full width at half maximum (FWHM) values of the etched sample compared to the as-grown [50,51].

The formation of GaN NWs during the metal assisted photochemical electroless etching take place through two main steps. Due to exposure of GaN layer to UV light in the presence of etching solution, electron holes pairs (e-h) starts to be generated in the interface between GaN layer and electrolyte constituting the first step. The photo-generated holes moves to the anode to oxidize the surface of GaN while electrons diffuse into the GaN bulk. A Ga_2O_3 layer will be formed in the anode with emission of N_2 gas following the reaction [38] "$2GaN + 6H^+ + 3H_2O \rightarrow Ga_2O_3 + 6H^+ + N_2\uparrow$". Under the catalysis of Pt, the electrons are consumed by H_2O_2 [52]. Simultaneously, a reduction reaction of H_2O_2 at the platinum will take place and will play the role of cathode, where, water will be generated following the equation "$H_2O_2 + 2H^+ \rightarrow 2H_2O + 2H^+$". The reaction of HF with the formed Ga_2O_3 will constitute the second step. A GaF_3 will be formed during the dissolution of the Ga_2O_3 oxide through the equation "$Ga_2O_3 + 6HF \rightarrow 2GaF_3 + 3H_2O$". This reaction will happen in the GaN grain surface, grain boundaries of GaN crystallites, and on the surface dislocations [53]. Etching for long time and after the formation of pores along the vertical (0 0 1) direction at the dislocation sites, GaN NWs structure will appear, where its length depends on the etching time [38].

Similar to the formation of GaN NWs [38,54,55], the synthesis of InGaN NWs can be interpreted by two main steps: During the first step, holes will be formed at the surface to generate dangling bonds through the reaction "$2InGaN + 12h^+ \rightarrow 2In^{3+} + 2Ga^{3+} + N_2\uparrow$" and support the anode reaction at the surface of InGaN. A nucleophilic species (such as OH) from the electrolyte will react with dangling bonds before its saturation with electrons from the semiconductor following the two equations [39]:

$$2H_2O + 2e \rightarrow 2OH^- + H_2$$

$$2In^{3+} + 2Ga^{3+} + 12OH^- \rightarrow In_2O_3 + Ga_2O_3 + 6H_2O$$

The dissolution of the formed In_2O_3 in HF in the solution will form the second step of the etching process. The etching of In_2O_3 will occur in the surface of InGaN crystal grain, on the grain boundaries of InGaN crystallites and at the surface dislocations similar to GaN etching [53]. The formation of InGaN NWs will due to the dissolution of In_2O_3 and the formation of In_2O following the equation "$In_2O_3 + Ga_2O_3 + 8H^+ \rightarrow In_2O + Ga_2O + 4H_2O$". In this case, the anode will be the region, where In_2O was formed due to the dissolution of the In_2O_3 oxide [56].

To study the optical properties of GaN NWs and InGaN NWs, absorption, PL and PLE measurements were conducted on different samples. UV–VIS light absorption spectra of GaN NWs and InGaN NWs and the corresponding substrates are shown in Fig. 2 (a)-(b). A strong UV absorption band can be noted for GaN NWs, which is comparable to GaN film, as shown Fig. 2(a), indicating that the crystal quality of the NWs was maintained. In addition, the broader absorption edge observed for the GaN NWs compared to that of substrate is most likely due to non-uniform distribution of NWs [57]. The absorption spectra of the InGaN substrate and NWs are presented in Fig. 2(b), indicating strong absorption in the UV range, which gradually decreases in the visible range. The first absorption peak located around 360 nm corresponds to GaN layer underneath the InGaN layer, whereas the InGaN absorption region is located in between 450 nm and 525 nm. Furthermore, the absorption is sharper in the GaN NWs compared to the InGaN NWs. As expected that the absorption edge of InGaN nanowire is not sharp compared to GaN nanowires due to the InN compositional fluctuations [45,58]. This compositional fluctuation effect is observed clearly in the PLE spectrum of InGaN NWs (as shown in the inset of Fig. 2(d)), revealing two distinguished bandedges that can be due to different InN compositional fluctuation in different NWs.

The PL measurements of GaN NWs samples etched for 180 min and the as-grown GaN layer are in Fig. 2(c). It is evident that, for the as-grown GaN layer, the emission peaks are dominated by the bound exciton D0x located at 3.409 eV (363.7 nm), which is red-shifted by 1.7 nm to 3.425 eV (362 nm) for the GaN NWs sample etched for 180 min. Such peak shift of NWs peak compared to the bulk is expected due to the relaxation of compressive stress in NW structure that modifies the bandgap [59,60]. PLE spectrum taken at 500 nm shown in the inset of Fig. 2(c) indicates that the origin of peak emission produced by GaN NWs. The inset PLE signal at 360 nm is related to GaN NW bandgap and the one at 370 nm is related to the bandgap of the GaN layer underneath NW. It looks the PLE minor peaks are due to shallow defects related to Si dopants [61].

Fig. 2(d) shows the emission characteristics of $In_xGa_{1-x}N$ where x = 0.2. In the spectrum of the as-grown sample, a peak is observed at 2.604 eV (476 nm). The peak oscillations that accompany the band-edge peak may due to Fabry-Perot optical interference within the thin InGaN epilayer confined between GaN and air [13,52].

We note also in Fig. 2(d), a red-shift by 2.2 nm compared to InGaN layer. This red-shift can be attributed to the compressive strain relaxation [54]. However, the FWHM remains the same before and after etching that is ~17.5 nm, suggesting that the quality has been maintained after etching. During etching, the In concentration in the InGaN layer will decrease, contributing to strain relaxation [62]. The formation of NWs reduces the compressive stress due to the lattice mismatch between InGaN and GaN layers [63]. Indeed, photochemical etching occurs near the defects in the vicinity of the In ions and will affect the In component [64]. The two peaks at 460 and 470 nm are related to InGaN NWs as the PLE spectrum at InGaN emission peak shown in the inset indicates different bandedges due to the In compositional fluctuation [27,45]. Note that the PL GaN peak of the GaN layer underneath the NWs appears after etching.

To further study the NW optical properties, TRPL measurements were performed on InGaN and GaN NWs (Fig. 2(e)). The time decay spectrum of GaN NWs can be fitted well by two decay functions due to transitions of multiple centers.

The fitting was performed using biexponential function using $I(t) = A_{fast}\exp(-t/\tau_{fast}) + A_{slow}\exp(-t/\tau_{slow})$; where A_{fast} and A_{slow} are the fast and slow peak intensities at time t = 0, respectively, while τ_{fast} and τ_{slow} denote the decay lifetimes of the fast and slow components [44,45] non-exponential decay profile was used to fit the time decay of InGaN samples, which is commonly observed in InGaN-based structures due to spatial In concentration non-uniformity [65]. The slow lifetime is found to be around τ_{slow} = 107.5 ps, whereas the faster component is about τ_{fast} = 20.5 ps. Initially, the GaN signal decayed rapidly (τ_{fast} = 20.5 ps), followed by a slower relaxation of τ_{slow} = 95.3 ps. The lifetime of the InGaN NWs is shorter than that of GaN NWs. The lifetime of the InGaN

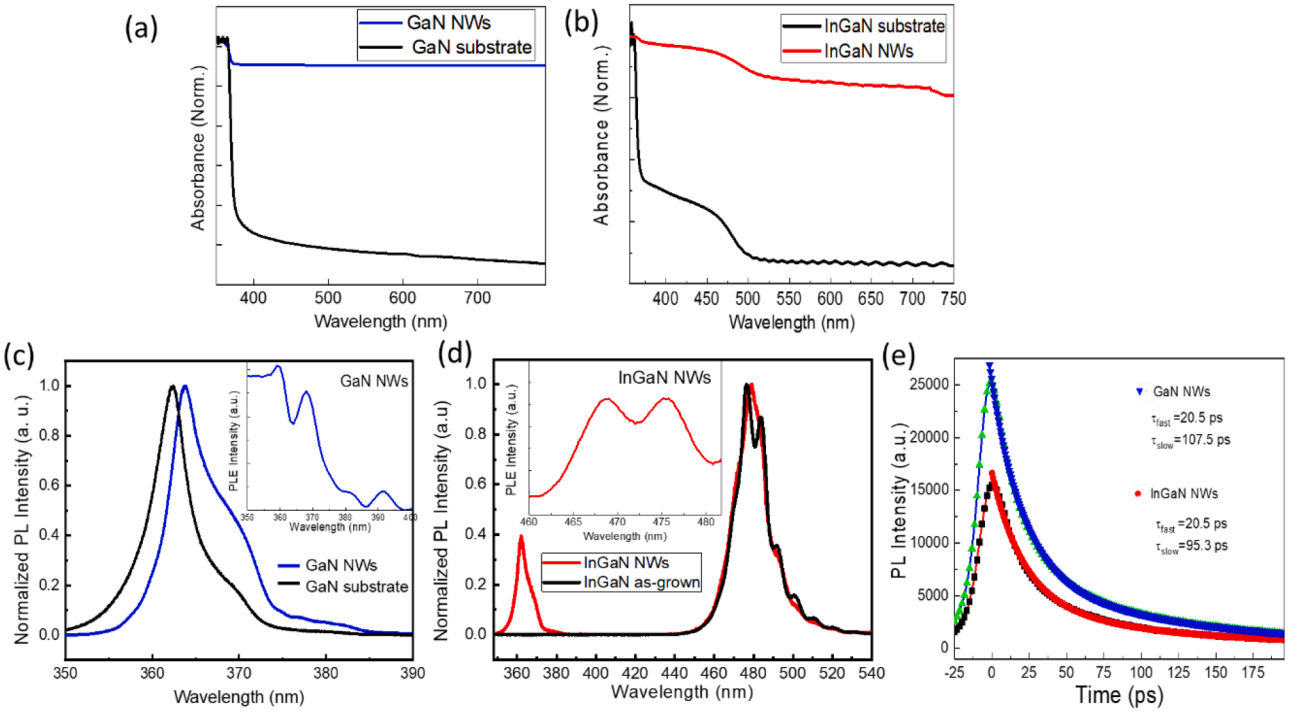

Fig. 2. Absorption spectra of (a) as-grown and GaN NWs and (b) as-grown InGaN and InGaN NWs. (c)-(d) PL spectra of as-grown InGaN and InGaN NWs samples etched for 30 min, respectively. The inset show the PLE spectra of NWs. (e) Time decay of PL measurements obtained at RT for (bleu triangle) wurtzite GaN NWs and (red circle) as-grown InGaN and InGaN NWs.

NWs is shorter than that of GaN NWs, suggesting a difference in the radiative and non-radiative contributions in each sample. However, it is known that, due to the InN fluctuation InGaN, the probability of exciton localization is higher in InGaN material more than that in GaN. For example, a similar fast lifetime trend has been observed in the InGaN NWs and has been attributed to the efficient radiative recombination of photoexcited carriers in the InGaN NWs [45].

DFT calculations

As a part of this investigation, we initially calculated the bulk lattice parameters of GaN and used the obtained values to construct the NW that was studied via DFT simulations to investigate the effect of InN cluster formation in the nanowire. The lattice parameters, a = 3.18 Å and c = 5.19 Å calculated for bulk GaN, are in good agreement with the experimental values (a = 3.1876 Å and c = 5.1846 Å) [45], thus confirming the accuracy of our calculations. The GaN NW was further optimized as it is very important to obtain a stable geometry owing to the large surface of NWs. In the relaxed GaN NW, the Ga–N bond length is compressed to 1.85 Å along the c-direction while the corresponding initial value before relaxation was 1.95 Å [66]. In the a-b plane, Ga–N bond length for the NW surface is 1.87 Å, whereas it increases to 1.92 Å for the inner atoms, which is very close to experimental value of bulk GaN. This distortion can be understood in terms of the reduced coordination number of atoms on the NW surface compared to the more bulk-like inner atoms. It is also worth noting that, in the GaN NW, the distance between the second nearest neighbor Ga atoms is 2.97 Å, compared to 3.21 Å obtained for the bulk. The Ga–N bond length distortion characterizing the NW is attributed to the increased surface-to-volume ratio, and the reduction in bondlength is in line with the

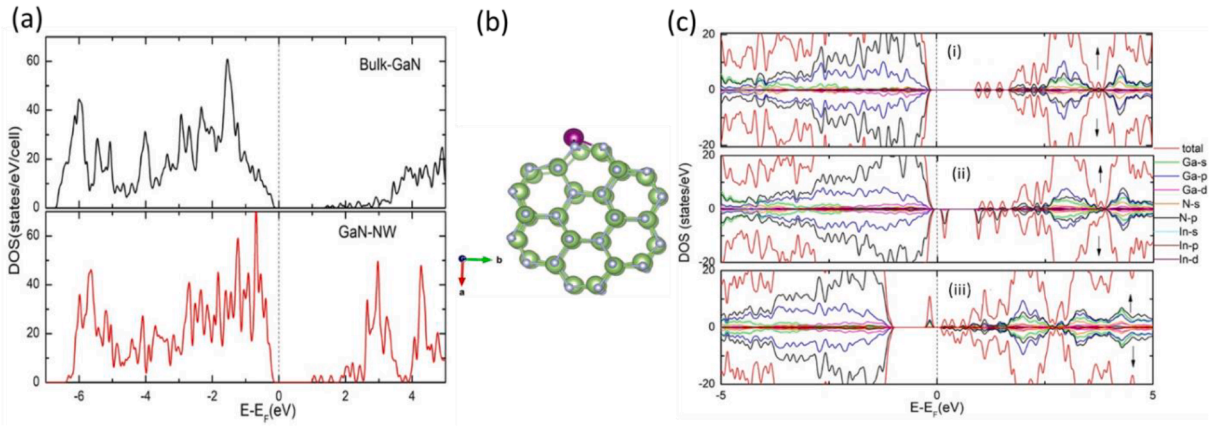

Fig. 3. (a) The total density of states of bulk GaN and GaN NW. (b) Optimized InGaN NW structure. The green, silver, and purple spheres represent Ga, N, and In atoms, respectively. (c) The total as well as the projected density of states of InGaN nanowire (i) defect free InGaN NW, (ii) InGaN NW in the presence of Ga vacancy, and (iii) N vacancy. The dotted line at the 0 represents the Fermi level.

values obtained in previous theoretical studies [42,46]. The density of states (DOS) of the bulk GaN and pristine GaN NW are shown in Fig. 3(a) to demonstrate the change in the electronic structure resulting from the dimension reduction from 3D to 1D.

To elucidate our experimental findings further, we introduced In and point defects into the NW and carried out optimization to obtain the most stable geometry. The optimized geometry of the In-doped NW is presented in Fig. 3(b). During the optimization, three scenarios were considered, namely (a) In atom substituted into the Ga site (InGa), (b) InGa in the presence of Ga vacancy (In-V_{Ga}), and (c) InGa in the presence of N vacancy (In-V_N). The formation energies (E_f; in eV) of these defects were calculated using Equation (1) [46] and are shown in Table 1.

$$E^f = \frac{(E^d_{total} - E(Ga_{48}N_{48}) + n_i\mu_i(Ga) - n_i\mu_i(In))}{n_i}$$

where the first two terms represent the total energy of the NW with In and the total energy of the pristine NW (without any defects), respectively. n_i shows the number of atoms removed/added for the respective elements; and μ_i is the chemical potential, which is the total energy calculated for the metallic Ga, In and atomic N. The obtained E^f values indicate that In can be easily substituted in the Ga site in the pristine NW, whereas the formation of defect complexes requires greater formation energy. It is worth mentioning that, in a previous study, we have shown that V_{Ga} is a more preferred defect in a GaN NW relative to V_N [46]. In this work, we also observed a similar trend for InGaN NWs. Interestingly, substituting In to the Ga site requires less formation energy than creating one V_{Ga} or V_N in the pristine GaN NW.

To explore the possibility of In atom clustering in the NW, we introduced one more In to create an In–In pair with different separation distances and calculated the formation energy, as presented in Table 2. As indicated by the reported data, In atoms prefer to stay further apart in NWs, as confirmed by slightly higher formation energies for those in closer proximity relative to those obtained for In atoms placed at a greater distance. However, when they are separated by about 10 Å, formation energy increases compared to the intermediate distances, corresponding to the effect of having an In atom in the close neighbourhood. We also introduced one V_{Ga} and V_N in the close vicinity of the In–In pair to gain insight into the formation of defect complexes. The findings indicate that the presence of In–In pair can reduce the formation energy of both native defects from 5.77 eV (for only V_{Ga}) and 6.42 eV (for only V_N) to 4.66 eV (lowest value, for In − In + 1 V_{Ga}) and 5.05 eV (lowest value, for In − In + 1 V_N), emphasizing the probability of their coexistence with In dopants, however, V_{Ga} is more preferred. This property can reflect in the changes in the NW electronic structure.

To explain some of our experimental results, we further calculated the density of states (DOS) to analyze the effect of In, as well as In-V_{Ga} and In-V_N complexes, in the NW and the findings are presented in Fig. 3. It can be seen that, in the absence of other defects, the In-doped GaN NW (Fig. 3(c)-i) is showing semiconducting behaviour. Fig. 3(c)-ii shows that the presence of V_{Ga} along with In induces additional states near the middle of the bandgap, mainly comprising of N-*p* states in the minority spin channel near the fermi level (E_F), indicating the possibility of hybridization with the defect states. In addition, a slight shift in the valence band maximum (VBM) toward the high-energy region and the presence of an acceptor state in the bandgap is noted in the presence of V_{Ga}. A similar observation has been reported for V_{Ga} in bulk GaN, where the presence of V_{Ga} was shown to increase the acceptor density [59]. Concurrent presence of V_N and In shifts the VBM to lower energies (Fig. 3(c)-iii). An additional level, which is a shallow donor level, is produced below the EF, whereby the unfilled electron state can increase the conductivity of the NW [67,68]. A comparison of the experimentally obtained bandgaps of bulk GaN and bulk InGaN shows that InGaN produces a peak at 2.60 eV owing to the presence of In (at 20% concentration). However, while comparing InGaN NWs to InGaN bulk, our DFT calculation reveals that the bandgap energy increased from 2.60 eV for bulk to 2.62 eV for NWs, suggesting that both V_N and In are involved in shifting the VBM to lower energies, thereby increasing the bandgap (Fig. 3(c)-iii). Practically the vacancy density and InN concentration can be controlled during the growth of InGaN/GaN epilayers before etching.

Table 1
The formation energy of In with and without V_{Ga} and VN in GaN NW. The formation energy of V_{Ga} and VN in the pristine GaN NW is also given for comparison.

Configuration	E_f (eV)
$Ga_{47}N_{48}In$ (One In)	1.40
$Ga_{46}N_{48}In$ (In + V_{Ga})	4.55
$Ga_{47}N_{48}$ (only V_{Ga})	5.77
$Ga_{47}N_{47}In$ (In + V_N)	8.51
$Ga_{48}N_{47}$ (only V_N)	6.42

Table 2
The formation energy of In − In pair and the separation distance between the In atoms. Formation energy is also shown for V_{Ga} and VN in the vicinity of the In-In pair.

Distance (Å)	Formation energy (eV)		
	In − In	In − In + 1 V_{Ga}	In − In + 1 V_N
3.34	1.09	4.93	5.16
6.17	1.05	5.62	6.42
7.38	1.05	5.74	6.28
10.38	1.08	4.66	5.05

Our DFT study showed that InGaN NWs were energetically stable and were associated with a change in lattice parameter along the c-direction, compared to the corresponding bulk value, thus supporting the existence of compressive stress observed experimentally. Further, electronic structure calculations were performed to analyse the effects of In and V_{Ga}, as well as V_N, in the InGaN NWs. The DOS calculations showed that the presence of V_N alters the NW conductivity properties, while V_{Ga} introduces defect states in InGaN NW.

Conclusion

In this work, GaN and InGaN NWs were synthesized by the metal-assisted photochemical electroless etching method. Both NWs exhibited PL shifts compared to the corresponding bulk material, which is attributed to the relaxation of compressive stress. DFT results indicates the segregation of In is not preferred in NW structure, indicating that InN fluctuation decreases in InGaN NWs compared to bulk. Moreover, DFT calculations showed that it is possible to tune the NW conduction/optical properties by a careful selection of In and other vacancy defects. These low-cost nanowires will have potential applications in light-emitting diodes, lasers, photodetectors, PEC water splitting and photoelectrodes.

Authorship contribution statement

S.A. Aravindh performs DFT simulations, A. Najar synthesis samples and performs SEM, XRD and PL measurements, B. Xin & S. Mitra performs absorption and PLE measurements, S.A. Aravindh, A. Najar and I. Roqan analyze the results and wrote the manuscript.

Declaration of Competing Interest

The authors declare that they have no known competing financial interests or personal relationships that could have appeared to influence the work reported in this paper.

Acknowledgement

This work was supported by UAE University under UPAR grant 31S306. The IBEX cluster, a part of KAUST supercomputing facilities was used to carry out the DFT calculations.

References

[1] Li Q, Wright JB, Chow WW, Luk TS, Brener I, Lester LF, et al. Single-mode GaN nanowire lasers. Opt Express 2012;20(16):17873–9. https://doi.org/10.1364/OE.20.017873.
[2] Schimpke T, Lugauer H-J, Avramescu A, Varghese T, Koller A, Hartmann J, Ledig J, Waag A, Strassburg M, Position-controlled MOVPE growth and electro-optical characterization of core-shell InGaN/GaN microrod LEDs, Light-Emitting Diodes: Materials, Devices, and Applications for Solid State Lighting XX, International Society for Optics and Photonics, 2016, p. 97680T doi: 10.1117/12.2214122.
[3] Nami M, Rashidi A, Monavarian M, Mishkat-Ul-Masabih S, Rishinaramangalam AK, Brueck SR, et al. Electrically injected GHz-class GaN/InGaN core-shell nanowire-based μLEDs: carrier dynamics and nanoscale homogeneity. ACS Photonics 2019;6(7):1618–25. https://doi.org/10.1021/acsphotonics.9b00639.
[4] Kishino K, Nagashima K, Yamano K. Monolithic integration of InGaN-based nanocolumn light-emitting diodes with different emission colors. Appl Phys Express 2012;6(1):012101. https://doi.org/10.7567/APEX.6.012101.
[5] Nami M, Stricklin IE, DaVico KM, Mishkat-Ul-Masabih S, Rishinaramangalam AK, Brueck S, et al. Carrier dynamics and electro-optical characterization of high-performance GaN/InGaN core-shell nanowire light-emitting diodes. Sci Rep 2018;8(1):1–11. https://doi.org/10.1038/s41598-017-18833-6.
[6] Tchernycheva M, Neplokh V, Zhang H, Lavenus P, Rigutti L, Bayle F, et al. Core–shell InGaN/GaN nanowire light emitting diodes analyzed by electron beam induced current microscopy and cathodoluminescence mapping. Nanoscale 2015;7(27):11692–701. https://doi.org/10.1039/C5NR00623F.
[7] Cademartiri L, Ozin GA. Ultrathin nanowires—a materials chemistry perspective. Adv Mater 2009;21(9):1013–20. https://doi.org/10.1002/adma.200801836.
[8] Lieber CM. Nanoscale Science and Technology: Building a Big Future from Small Things. MRS Bull 2003;28(7):486–91. https://doi.org/10.1557/mrs2003.144.
[9] Pauzauskie PJ, Yang P. Nanowire photonics. Mater Today 2006;9(10):36–45. https://doi.org/10.1016/S1369-7021(06)71652-2.
[10] Najar A, Ajlani H, Charrier J, Lorrain N, Haesaert S, Oueslati M, et al. Optical study of erbium-doped-porous silicon based planar waveguides. Physica B 2007;396(1–2):145–9. https://doi.org/10.1016/j.physb.2007.03.034.
[11] Najar A, Charrier J, Ajlani H, Lorrain N, Elhouichet H, Oueslati M, et al. Optical properties of erbium-doped porous silicon waveguides. J Lumin 2006;121(2):245–8. https://doi.org/10.1016/j.jlumin.2006.08.072.
[12] Najar A, Charrier J, Ajlani H, Lorrain N, Haesaert S, Oueslati M, et al. Optical gain at 1.53 μm in Er3+–Yb3+ co-doped porous silicon waveguides. Mater Sci Eng, B 2008;146(1–3):260–3. https://doi.org/10.1016/j.mseb.2007.07.085.
[13] Muhammed M, Roldan M, Yamashita Y, Sahonta S-L, Ajia IA, Iizuka K, et al. High-quality III-nitride films on conductive, transparent (2¯01)-oriented β-Ga 2 O 3 using a GaN buffer layer. Sci Rep 2016;6:29747. https://doi.org/10.1038/srep29747.
[14] Razeghi M. III-nitride optoelectronic devices: from ultraviolet toward terahertz. IEEE Photonics J 2011;3(2):263–7. https://doi.org/10.1109/JPHOT.2011.2135340.
[15] Wu J. When group-III nitrides go infrared: new properties and perspectives. J Appl Phys 2009;106(1):5. https://doi.org/10.1063/1.3155798.
[16] Lu P, Liang D, Chen Y, Zhang C, Quhe R, Wang S. Closing the bandgap for III-V nitrides toward mid-infrared and THz applications. Sci Rep 2017;7(1):1–10. https://doi.org/10.1038/s41598-017-11093-4.
[17] Kim HM, Lee H, Kim SI, Ryu SR, Kang TW, Chung KS. Formation of InGaN nanorods with indium mole fractions by hydride vapor phase epitaxy. Phys Status Solidi (b) 2004;241(12):2802–5. https://doi.org/10.1002/pssb.200405043.
[18] Stoica T, Sutter E, Meijers RJ, Debnath RK, Calarco R, Lüth H, et al. Interface and wetting layer effect on the catalyst-free nucleation and growth of GaN nanowires. Small 2008;4(6):751–4. https://doi.org/10.1002/smll.200700936.
[19] Jiang B, Zhang C, Wang X, Xue F, Park MJ, Kwak JS, et al. Effects of reduced exciton diffusion in InGaN/GaN multiple quantum well nanorods. Opt Express 2012;20(12):13478–87. https://doi.org/10.1364/OE.20.013478.
[20] Hersee SD, Rishinaramangalam AK, Fairchild MN, Zhang L, Varangis P. Threading defect elimination in GaN nanowires. J Mater Res 2011;26(17):2293. https://doi.org/10.1557/jmr.2011.112.
[21] Najar A, Elhouichet H, Lorrain N, Oueslati M. Excitation mechanisms and localization sites of erbium-doped porous silicon. Appl Surf Sci 2006;252(16):5808–13. https://doi.org/10.1016/j.apsusc.2005.07.071.
[22] Calarco R, Meijers RJ, Debnath RK, Stoica T, Sutter E, Lüth H. Nucleation and growth of GaN nanowires on Si (111) performed by molecular beam epitaxy. Nano Lett 2007;7(8):2248–51. https://doi.org/10.1021/nl0707398.
[23] Nami M, Rishinaramangalam A, Feezell D. Analysis of light extraction efficiency for gallium nitride-based coaxial microwall light-emitting diodes. Phys Status Solidi (c) 2014;11(3–4):766–70. https://doi.org/10.1002/pssc.201300456.
[24] Najar A, Omi H, Tawara T. Scandium effect on the luminescence of Er-Sc silicates prepared from multi-nanolayer films. Nanoscale Res Lett 2014;9(1):1–6. https://doi.org/10.1186/1556-276X-9-356.
[25] Qamhieh N, Najar A, Qamhieh Z, Aziz BA, Mansour A, Alghoul I. Synthesis and characterization of a perovskite film for solar cells applications. Optik 2018;171:648–51. https://doi.org/10.1016/j.ijleo.2018.05.066.
[26] Najar A, Omi H, Tawara T. Effect of structure and composition on optical properties of Er-Sc silicates prepared from multi-nanolayer films. Opt Express 2015;23(6):7021–30. https://doi.org/10.1364/OE.23.007021.
[27] Alfaraj N, Mitra S, Wu F, Ajia IA, Janjua B, Prabaswara A, et al. Photoinduced entropy of InGaN/GaN pin double-heterostructure nanowires. Appl Phys Lett 2017;110(16):161110. https://doi.org/10.1063/1.4981252.
[28] Seo HW, Bae SY, Park J, Yang H, Park KS, Kim S. Strained gallium nitride nanowires. J Chem Phys 2002;116(21):9492–9. https://doi.org/10.1063/1.1475748.
[29] Kuykendall T, Ulrich P, Aloni S, Yang P. Complete composition tunability of InGaN nanowires using a combinatorial approach. Nat Mater 2007;6(12):951–6. https://doi.org/10.1038/nmat2037.
[30] Zhong Z, Qian F, Wang D, Lieber CM. Synthesis of p-type gallium nitride nanowires for electronic and photonic nanodevices. Nano Lett 2003;3(3):343–6. https://doi.org/10.1021/nl034003w.
[31] Kim H-M, Lee W, Kang T, Chung K, Yoon CS, Kim CK. InGaN nanorods grown on (1 1 1) silicon substrate by hydride vapor phase epitaxy. Chem Phys Lett 2003;380(1–2):181–4. https://doi.org/10.1016/j.cplett.2003.09.020.
[32] Najar A, Charrier J, Pirasteh P, Sougrat R. Ultra-low reflection porous silicon nanowires for solar cell applications. Opt Express 2012;20(15):16861–70. https://doi.org/10.1364/OE.20.016861.
[33] Hersee SD, Sun X, Wang X. The controlled growth of GaN nanowires. Nano Lett 2006;6(8):1808–11. https://doi.org/10.1021/nl060553t.
[34] Nami M, Eller RF, Okur S, Rishinaramangalam AK, Liu S, Brener I, et al. Tailoring the morphology and luminescence of GaN/InGaN core–shell nanowires using bottom-up selective-area epitaxy. Nanotechnology 2016;28(2):025202. https://doi.org/10.1088/0957-4484/28/2/025202.
[35] Najar A, Slimane A, Hedhili MN, Anjum D, Sougrat R, Ng T, et al. Effect of hydrofluoric acid concentration on the evolution of photoluminescence characteristics in porous silicon nanowires prepared by Ag-assisted electroless etching method. J Appl Phys 2012;112(3):033502. https://doi.org/10.1063/1.4740051.
[36] Najar A, Gerland M, Jouiad M. Porosity-induced relaxation of strains in GaN layers studied by means of micro-indentation and optical spectroscopy. J Appl Phys 2012;111(9):093513. https://doi.org/10.1063/1.4710994.
[37] Najar A, Shafa M, Anjum D. Synthesis, optical properties and residual strain effect of GaN nanowires generated via metal-assisted photochemical electroless etching. RSC Adv 2017;7(35):21697–702. https://doi.org/10.1039/C7RA02348K.
[38] Najar A, Jouiad M. Synthesis of InGaN nanowires via metal-assisted photochemical electroless etching for solar cell application. Sol Energy Mater Sol Cells 2018;180:243–6. https://doi.org/10.1016/j.solmat.2017.06.008.
[39] Fang D, Rosa A, Frauenheim T, Zhang R. Band gap engineering of GaN nanowires by surface functionalization. Appl Phys Lett 2009;94(7):073116. https://doi.org/10.1063/1.3086316.
[40] Wang Q, Sun Q, Jena P. Ferromagnetism in Mn-doped GaN nanowires. Phys Rev Lett 2005;95(16):167202. https://doi.org/10.1103/PhysRevLett.95.167202.
[41] Aravindh SA, Cao W, Alatalo M, Huttula M. Ab initio study of hydrogen sensing in Pd and Pt functionalized GaN [0001] nanowires. Appl Surf Sci 2020:146019. https://doi.org/10.1016/j.apsusc.2020.146019.
[42] Kresse G, Furthmüller J. Efficient iterative schemes for ab initio total-energy calculations using a plane-wave basis set. Phys Rev B 1996;54(16):11169–86. https://doi.org/10.1103/PhysRevB.54.11169.
[43] Assa Aravindh SD, Schwingenschloegl U, Roqan IS. Defect induced d 0 ferromagnetism in a ZnO grain boundary. J Chem Phys 2015;143(22):224703. https://doi.org/10.1063/1.4936659.
[44] Ajia IA, Yamashita Y, Lorenz K, Muhammed M, Spasevski L, Almalawi D, et al. GaN/AlGaN multiple quantum wells grown on transparent and conductive (-201)-oriented β-Ga2O3 substrate for UV vertical light emitting devices. Appl Phys Lett 2018;113(8):082102. https://doi.org/10.1063/1.5025178.
[45] Ajia IA, Edwards PR, Pak Y, Belekov E, Roldan MA, Wei N, et al. Generated carrier dynamics in V-pit-enhanced InGaN/GaN light-emitting diode. ACS Photonics 2017;5(3):820–6. https://doi.org/10.1021/acsphotonics.7b00944.
[46] Blöchl PE. Projector augmented-wave method. Phys Rev B 1994;50(24):17953–79. https://doi.org/10.1103/PhysRevB.50.17953.
[47] Dudarev SL, Botton GA, Savrasov SY, Humphreys CJ, Sutton AP. Electron-energy-loss spectra and the structural stability of nickel oxide: an LSDA+U study. Phys Rev B 1998;57(3):1505–9. https://doi.org/10.1103/PhysRevB.57.1505.
[48] Zhang J, Zhang L, Wang X, Liang C, Peng X, Wang Y. Fabrication and photoluminescence of ordered GaN nanowire arrays. J Chem Phys 2001;115(13):5714–7. https://doi.org/10.1063/1.1407005.
[49] Qu Y, Zhou H, Duan X. Porous silicon nanowires. Nanoscale 2011;3(10):4060–8. https://doi.org/10.1039/C1NR10668F.
[50] Radzali R, Hassan Z, Zainal N, Yam F. Nanoporous InGaN prepared by KOH electrochemical etching with different light sources. Microelectron Eng 2014;126:107–12. https://doi.org/10.1016/j.mee.2014.06.027.
[51] Zhang M-R, Jiang Q-M, Zhang S-H, Wang Z-G, Hou F, Pan G-B. Fabrication of gallium nitride nanowires by metal-assisted photochemical etching. Appl Surf Sci 2017;422:216–20. https://doi.org/10.1016/j.apsusc.2017.06.014.
[52] Chen D, Xiao H, Han J. Nanopores in GaN by electrochemical anodization in hydrofluoric acid: Formation and mechanism. J Appl Phys 2012;112(6):064303. https://doi.org/10.1063/1.4752259.

[53] Radzali R, Zainal N, Yam F, Hassan Z. Nanoporous InGaN of high In composition prepared by KOH electrochemical etching. Mater Sci Semicond Process 2013;16 (6):2051–7. https://doi.org/10.1016/j.mssp.2013.07.035.
[54] Lu Y, Cong G, Liu X, Lu D-C, Zhu Q, Wang X, et al. Growth of crack-free GaN films on Si (111) substrate by using Al-rich AlN buffer layer. J Appl Phys 2004;96(9): 4982–8. https://doi.org/10.1063/1.1787588.
[55] Dorogan V, Vieru T, Tigyneanu I, Hartnagel H, Mutamba C, Sturza R. Photoelectrochemical etching of GaN-AlGaN heterostructures formed on sapphire substrates, Moldavian J Phys Sci 1(2) (2002) 156-159. doi: http://nano.asm.md/ru/pages/itemView/31.
[56] Pimputkar S, Suihkonen S, Imade M, Mori Y, Speck J, Nakamura S. Free electron concentration dependent sub-bandgap optical absorption characterization of bulk GaN crystals. J Cryst Growth 2015;432:49–53. https://doi.org/10.1016/j.jcrysgro.2015.09.016.
[57] Flemban TH, Singaravelu V, Devi AAS, Roqan IS. Homogeneous vertical ZnO nanorod arrays with high conductivity on an in situ Gd nanolayer. RSC Adv 2015;5 (115):94670–8. https://doi.org/10.1039/C5RA19798H.
[58] Wu F, Sun H, AJia IA, Roqan IS, Zhang D, Dai J, Chen C, Feng ZC, Li X. Significant internal quantum efficiency enhancement of GaN/AlGaN multiple quantum wells emitting at~ 350 nm via step quantum well structure design. J Phys D Appl Phys 2017;50(24):245101. https://doi.org/10.1088/1361-6463/aa70dd.
[59] Hugues M, Shields P, Sacconi F, Mexis M, Auf der Maur M, Cooke M, et al. Strain evolution in GaN nanowires: from free-surface objects to coalesced templates. J Appl Phys 2013;114(8):084307. https://doi.org/10.1063/1.4818962.
[60] Callsen G, Kure T, Wagner MR, Butté R, Grandjean N. Excited states of neutral donor bound excitons in GaN. J Appl Phys 2018;123(21):215702. https://doi.org/10.1063/1.5028370.
[61] Hums C, Finger T, Hempel T, Christen J, Dadgar A, Hoffmann A, et al. Fabry-Perot effects in In Ga N/ Ga N heterostructures on Si-substrate. J Appl Phys 2007;101(3): 033113. https://doi.org/10.1063/1.2434010.
[62] Cao D, Xiao H, Gao Q, Yang X, Luan C, Mao H, et al. Fabrication and improved photoelectrochemical properties of a transferred GaN-based thin film with InGaN/GaN layers. Nanoscale 2017;9(32):11504–10. https://doi.org/10.1039/C7NR03622A.
[63] Ebaid M, Kang J-H, Yoo Y-S, Lim S-H, Cho Y-H, Ryu S-W. Vertically aligned InGaN nanowires with engineered axial In composition for highly efficient visible light emission. Sci Rep 2015;5:17003. https://doi.org/10.1038/srep17003.
[64] Tamboli A, Hu EL, Schmidt MC, Nakamura S, DenBaars SP, Photoelectrochemical etching of P-type semiconductor heterostructures, US Patents, US8053264B2, 2011.
[65] Porowski S. Bulk and homoepitaxial GaN-growth and characterisation. J Cryst Growth 1998;189:153–8. https://doi.org/10.1016/S0022-0248(98)00193-6.
[66] Oila J, Saarinen K, Wickenden A, Koleske D, Henry R, Twigg M. Ga vacancies and grain boundaries in GaN. Appl Phys Lett 2003;82(7):1021–3. https://doi.org/10.1063/1.1542946.
[67] Zhang Z, Schwingenschlögl U, Roqan IS. Possible mechanism for d 0 ferromagnetism mediated by intrinsic defects. RSC Adv 2014;4(92):50759–64. https://doi.org/10.1039/C4RA06237J.
[68] Zhang Z, Schwingenschlögl U, Roqan IS. Vacancy complexes induce long-range ferromagnetism in GaN. J Appl Phys 2014;116(18):183905. https://doi.org/10.1063/1.4901458.